Performance based evaluation of steel special moment resisting frames with viscous dampers

H. Kit Miyamoto[1, 2)], Amir S. Gilani[1)], and Akira Wada[2)]
1. Miyamoto International, Sacramento, US
2. Tokyo Institute of Technology, Japan

ABSTRACT: Viscous dampers provide an efficient mean of controlling drift in steel moment-resisting structures. In design, damping devices are added to steel moment frames that have been designed using the code strength procedures and utilize ductile beam-to-column connections such as reduced beams. Construction savings are realized in this approach, owning to smaller frame sizes and reduced foundation work. Experience has shown that such approach is reliable and has a high confidence of meeting the performance goals at design or maximum earthquakes (DE and MCE, respectively). The models of viscous dampers used to date do not incorporate the damper limit states. Such limit states can have a significant influence on the response of the moment frames. To address this issue, a refined model of viscous dampers has been developed. The model incorporates both displacement and force limit states. Simulations were conducted to check the limit state activation for the model. Experimental data were then used to verify the accuracy of such limit states. Finally, a one story building was analyzed to assess the effect of limit states on the building response.

1 INTRODUCTION

Viscous dampers were originally developed as shock absorbers for the defense and aerospace industries. In recent years, they have been used extensively for seismic application for both new and retrofit construction. During seismic events, the devices become active and the seismic input energy is used to heat the fluid and is thusly dissipated. Subsequent to installation, the dampers require minimal maintenance. They have been shown to possess stable and dependable properties for design earthquakes. Figure 1 depicts the application of dampers to a new building in California (Miyamoto and Gilani, 2008).

Figure 1. steel moment frame with dampers

To date, no comprehensive study has been undertaken to investigate limit state of viscous dampers and to characterize the effect on the building once a damper limit state is reached. This paper presents some preliminary result from a comprehensive research currently underway to address this issue. Since dampers are ideal for drift control in steel moment frame buildings, the investigation is focused on this type of construction.

2 MODELING OF VISCOUS DAMPERS

2.1 *Component of viscous dampers*

Viscous dampers consist of a cylinder and a stainless steel piston. The cylinder is filled with incompressible silicone fluid. The damper is activated by the flow of silicone fluid between chambers at opposite ends of the unit, through small orifices. Figure 2 shows the damper cross section.

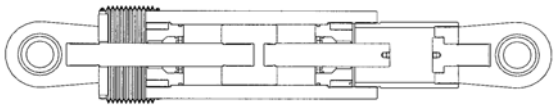

Figure 2. Viscous damper cross section

2.2 *Maxwell model*

In most applications, the dampers are modeled as simple Maxwell model of Figure 3 The viscous damper itself is modeled as a dashpot in series with the elastic driver brace member.

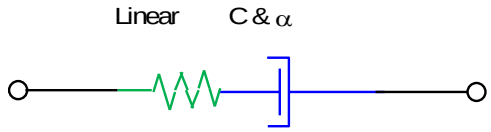

Figure 3. Maxwell model

Such model is adequate for most design applications, but is not sufficiently refined for collapse evaluation. In particular, force and displacement limit states are unaccounted.

2.3 *Damper limit states*

Although dampers are comprised of many parts, the limit states are governed by a few elements. The dampers bottoms out, once the piston motion reaches its available stroke. This is the stroke limit and results in transition from viscous damper to a steel brace with stiffness equal to that of the cylinder wall. The force limit states in compression and tension are governed by the buckling capacity of the driver brace and the tensile capacity of the piston rod, respectively.

2.4 *Refined model for viscous dampers*

Figure 4 presents the proposed refined model for viscous dampers. This model is developed to incorporate the pertinent limit states and consists of five components. The constitutive relation for the refined model in terms of force, velocity, and displacement is listed in (Eq 1)

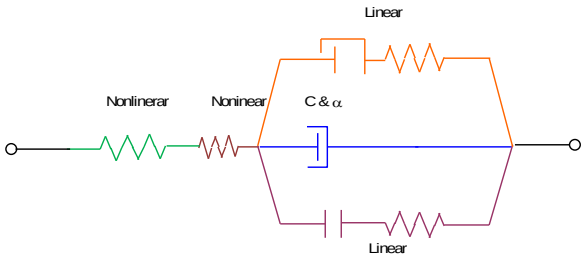

Figure 4. Refined model

$$\Delta u = \frac{\Delta F}{K_D(u)} + \frac{\Delta F}{K_P(u)} + \begin{cases} \frac{\Delta F}{K_C} \ldots\ldots |u| > u_{\max} \\ \operatorname{sgn}(F)\frac{1}{C^{\alpha}}\int |F|^{1/\alpha}\, dt \end{cases}$$

$$\Delta F = 0 \ldots |F| \geq F u_P \qquad (1)$$

The damper components are as following:

- The driver (KD), used to attach the damper to the gust plates at the beam-to-column connection, is modeled as a nonlinear spring.
- The piston rod (KP) and undercut is modeled as a nonlinear spring. The piston undercut is the machined down section between the end of the piston and the start of the piston male threaded part. In tension, the undercut section of the piston can yield and then fracture. The undercut area is approximately 80% of the full piston area. The piston ultimate strength is only 10% above yield. Hence, fracture quickly follows yielding.
- Dashpot (C and α) is used to model the viscous component.
- Gap element and linear springs (Kc) are used to model the limit state when the piston retraction equals the stroke (umax). The elastic stiffness depends on the damper construction and its cylinder properties.
- Hook elements and linear springs (Kc) are used to model the limit state when the piston extension reaches the damper stroke (umax). The stiffness is the same as that associated with the gap element.

2.5 *Response of the refined model*

In analysis, once the stroke limit is reached, the damper becomes numerically equivalent to a steel brace. Upon unloading, this process is reversed. When the force limit is reached, the entire damper is ineffective and thus permanently removed, even after unloading. The sudden transmissions between viscous damper, steel brace, and no members can impart large impact forces on the structure.

At the instant that the gap closes, the damper force is zero. However, as loading is continued, the unit displacement can increase due to deformation in the cylinder wall and thus velocity is non-zero. The result is a complex visco-elastic combination of Maxwell and Kelvin models,

At the large peaks, the damper force, which is algebraic sum of the force in the dashpot and the cylinder wall, can be smaller than the force resisted by the wall cylinders. This is because the forces in the viscous element and cylinder wall can be out-of-phase.

3 ANALYTICAL SIMULATIONS

3.1 *Overview*

To illustrate the response of the refined model and illustrate its capability to capture all the limit states, simulations were conducted. The damper was modeled in program OpenSees (PEER 2008) using the refined model. All analysis was conducted using a sinusoidal displacement loading function; see Figure 5.

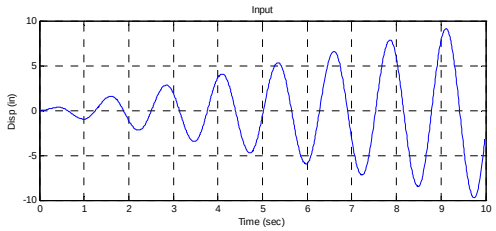

Figure 5. Input function for 150-kip damper simulation

The damper used in simulation is the 700-kN unit and has a constitutive relation (force in kN and velocity in mm/sec) of Eq. 2

$$F = 88\,\mathrm{sgn}(v)|v|^{0.3} \quad (2)$$

3.2 *Force limit state of piston fracture*

This simulation was conducted to investigate the damper response for the limit state of piston undercut fracture. The stroke was artificially set to be large enough to ensure that the damper did not bottom out in tension. The response is shown in Figure 6. Note that the force transmitted by the cylinder walls is zero since the damper has not bottomed out. Once the piston undercut reaches its tensile capacity, the damper element is automatically removed from the simulation and the forces drop to zero.

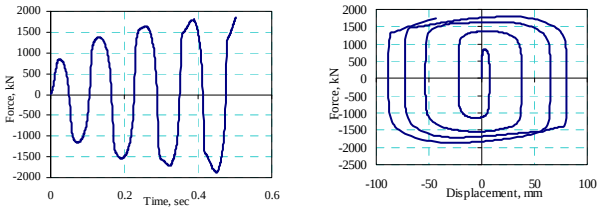

a. Damper d. Damper hysteresis

Figure 6. Response of damper when undercut fractures

3.3 *Stroke limit states*

This simulation was conducted to investigate the damper response for the limit state when the stroke limit in extension and retraction are reached. The undercut tensile and piston and driver brace compressive capacity were artificially set to be large enough for these members to remain elastic. The response is shown in Figure 7. Note that the force transmitted by the cylinder walls is non-zero, once the stoke limit in either tension or compression is reached. The total force transmitted by the damper is the sum of displacement-proportional elastic force in the cylinder wall and velocity-proportional force in the viscous component (Kelvin model). Once the stoke limit is reached, the velocity drops to zero and thus the force in the viscous element is zero. In structural applications, this will tend to translate to increased lateral stiffness and decreased effective damping ratio.

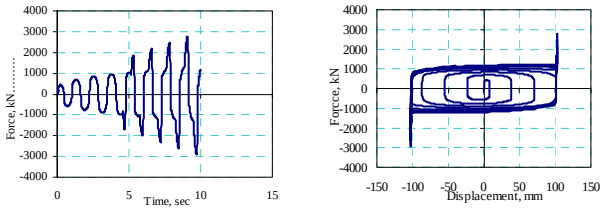

a. Damper b. Damper hysteresis

Figure 7. Response of damper when damper bottoms out

3.4 *Displacement and force limits*

The stroke limit is reached first. If the loading is increased, then the driver will buckle in tension or undercut will yield and fracture in tension.

This simulation was conducted to investigate the damper response for the limit state of piston fracture following bottoming out of damper at full extension. The response is shown in Figure 8. At 4.5 sec in the response, the piston extension reaches the stroke limit and the damper bottoms out. At this point, velocity is zero and thus the force in the viscous element drops to zero. The damper acts as a elastic brace. The undercut yields but does not fracture. Loading is then reversed. This results in the disengagement of cylinder walls, and re-loading of the viscous component. At 5.3 sec, piston bottoms out again. The damper again becomes an elastic brace. Loading is increased further resulting in fracture of undercut. The entire damper is now ineffective and removed.

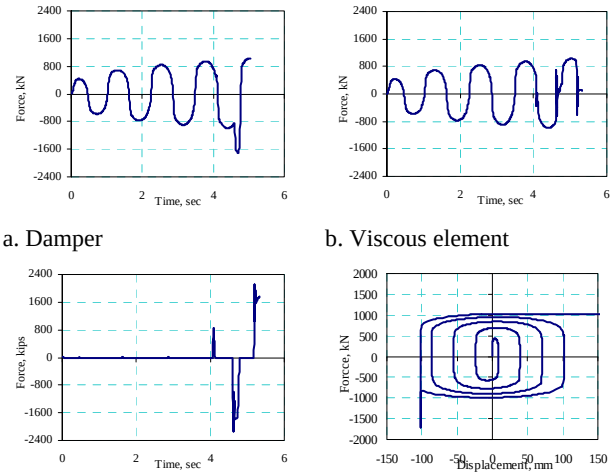

a. Damper b. Viscous element

c. Cylinder walls d. Damper hysteresis

Figure 8. Response of damper when damper bottoms out followed by the piston fracture

3.5 *Response to Earthquake acceleration*

The damper was next subjected to the Kobe record to assess its performance of the damper. The unsealed input acceleration is shown in Figure 9a, and was used as acceleration input along the axis of the damper element. Figure 9b presents the response at 100% intensity. Note that the response is that of the pure viscous damper and no limit states are reached. Next the record was amplified to 125% and

the response is shown in Figure 9c. Even such modest amplification, resulted in the damper reaching its displacement limit and bottoming out in both tension and compression. Once damper bottomed, large elastic forces (twice the maximum viscous force) were generated and which must be resisted by steel members in structural applications. Finally, the force limit state was reached when the record was amplified by 175%; see Figure 9d. This is not a large scaling. The damper bottomed out in compression twice, followed by bottoming in tension which leads to the yielding and fracture of piston undercut. After this point, the damper is completely ineffective. In structural applications, this implies removal of beneficial supplementary energy from the system.

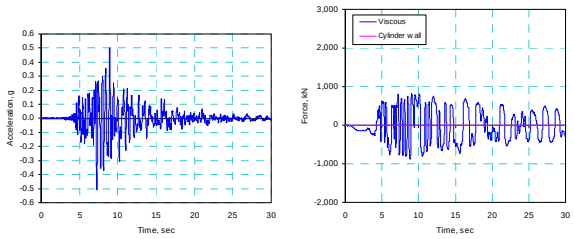

a. Input acceleration b. Response, 100% event

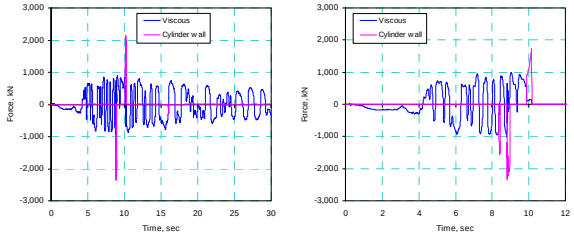

c. Response, 125% event d. Response, 175% event

Figure 9. Response of damper to Kobe record

4 CORRELATION WITH TEST RESULTS

Experimental data from a damper (Taylor, 2008) was used to assess the accuracy of the refined mathematical model of dampers. This damper was laboratory tested and was subjected to large velocity and displacement pulses in succession and experienced several of its limit states. This damper had a nominal capacity of 2000 kN at a velocity of 330 mm/sec. It had a stroke of 140 mm, a damping constant of 3.5 kN/mm and a damping exponent of 0.5. Hence its constitutive relation (force in kips and velocity in in./sec), in the design range, is written as in Eq 3.

$$F = 3.5\,\mathrm{sgn}(v)|v|^{0.5} \quad (3)$$

The damper was placed in the test rig and subject to a displacement loading history. The unit was placed with its piston extended to within 10 mm of the stroke limit prior to start of the displacement cycles.

The experimental displacement, velocity, and force responses are presented as solid lines in 10a through 10c, respectively. The damper limit states are identified in this figure.

At 4.3 sec, the unit was pulled in tension at 910 mm/sec and stopped just before it bottomed. This large velocity was close to 300% of its nominal design. This resulted in the forces developed in the damper that exceeded the nominal value computed from the constitutive relation.

At 4.61 sec, the damper bottoms out in tension, resulting in sharp increase in the measured force. This is followed by tensile yielding. The displacement response after this point is nearly flat with a slight increase due to yielding.

Finally at 4.68 sec, fracture occurs and the damper load drops to zero. After this time, no force can be transferred by the damper.

The dashed lines in these figures represent the results obtain from simulation using the refined damper element. Good correlation is obtained between the experimental data and analytical simulations. The analytical model was able to capture the bottoming of the damper and tensile fracture correctly.

10d presents the force-displacement hysteresis and the dissipated energy in the damper. The analytical model captures the experimental responses closely, implying that the analytical model is able to reproduce the energy dissipation properties of the laboratory-tested unit.

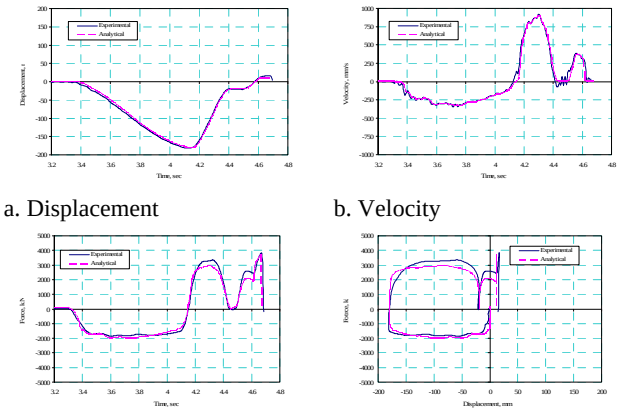

a. Displacement b. Velocity

c. Force d. Damper hysteresis

Figure 10. Experimental and analytical hysteresis

5 ANALYSIS PROCEDURE

5.1 *Ground motions*

The input histories used in analysis were based on the two components of the 22 far-filed (measured 10 km or more from fault rupture) NGA PEER (2008) records. These 44 records have been identified by ATC 63 (FEMA 2008) for collapse evaluation analysis. The selected 22 records correspond to a relatively large sample of strong recorded motions that are consistent with the code (ASCE/SEI 7) and are structure-type and site-hazard independent.

Figure 11 presents the acceleration response spectra for these records. The design MCE spectrum is shown as the dark solid line in the figure. For analysis, the 44 records were first normalized and then scaled. Normalization of the records was done to remove the record-to-record variation in intensity.

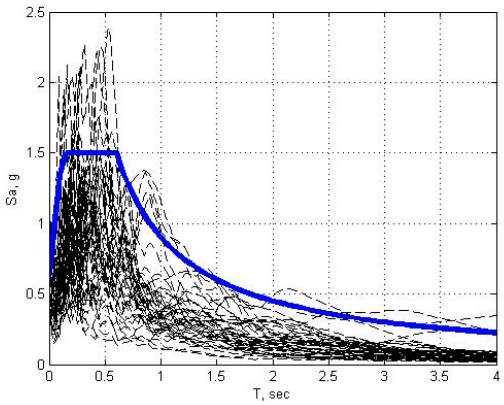

Figure 11. Response spectra of original records

5.2 *Software*

Program OpenSees (PEER 2005) was used to conduct the nonlinear analyses described in this paper. Pertinent model properties are listed here.

- Analytical models are two-dimensional
- Beam and column elements, are represented as one dimensional frame elements. The members are prismatic and linear.
- Material nonlinearity is represented by concentrated plastic hinges represented by RBS hinges placed at the center of the reduced section
- The damper element is represented by the refined model including the limit states.

5.3 *Methodology*

For collapse analysis, the normalized records are then scaled upward or downward to obtain data points for the nonlinear incremental dynamic analysis (IDA) simulations (Vamvatsikos and Cornell, 2004).

6 APPLICATION TO STEEL BUILDINGS

6.1 *General*

To illustrate the concepts described in this chapter, design and analysis of a single story structure with viscous damping was conducted. For comparative study, an undamped SMRF was also analyzed. The base of columns was assumed fixed.

The one-story frame is square in plan and measures 90 ft on each side. It is 13 ft tall. The structure has one interior SMRF on the perimeter on each side. One of the 30x13 ft frames was selected for design and analysis.

The frame was designed using the code provisions and special requirements for SMRFs. Both damped and undamped frames had similar member sizes.

For this structure, the fundamental period (T1) is 0.42 sec. The ASCE 7 maximum period used to compute base shear (Tmax) is 0.31 second. This period is used for evaluation.

6.2 *Undamped structure*

Figure 12 presents the pushover curve for the undamped frame. The solid and dashed red lines correspond to the yield and maximum drift ratios. System ductility (μc) of more than 8 is computed. Using the building period and ductility, the spectral shape factor (SSF) is estimated at 1.34.

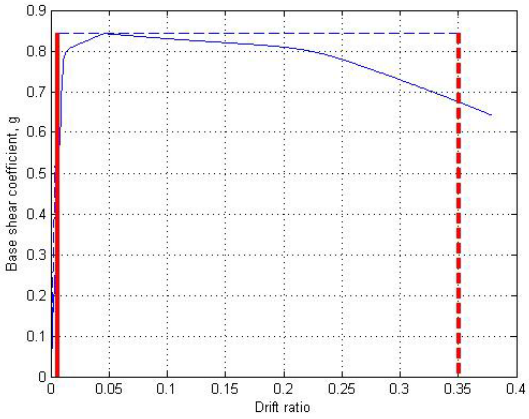

Figure 12. Pushover plot for case 1

Figure 13 presents the IDA plots for the undamped frame. The abscissa is the spectral acceleration, Sa, of input records at the maximum period as specified by ASCE/SEI 7 (ASCE 2005). The ordinates are the roof drift ratios. The solid and dashed red lines correspond to the MCE (SMT) and the median collapse capacity (SCT) for this case respectively.

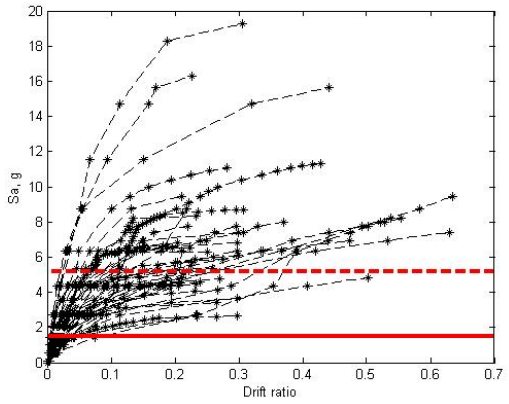

Figure 13. IDA plot for case 1

For this building, the collapse margin ratio is computed to equal 3.46. The adjusted collapse mar-

gin ratio (ACMR) is calculated by multiplying SSF by CMR and equals 3.8.

6.3 *Damped structure*

Figure 14 presents the pushover curve for the damped frame. The solid and dashed red lines correspond to the yield and maximum drift ratios. System ductility (μc) of 8.0 is computed. Using the building period and ductility, the spectral shape factor (SSF) is estimated at 1.34.

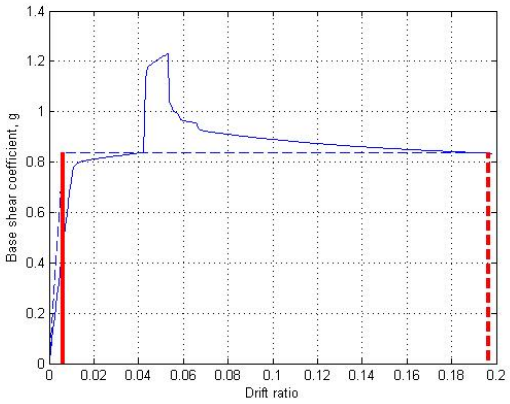

Figure 14. Static pushover curve for case 4

Figure 15 presents the IDA plots for the damped frame. The solid and dashed red lines correspond to the MCE (SMT) and the median collapse capacity (SCT) for this case respectively.

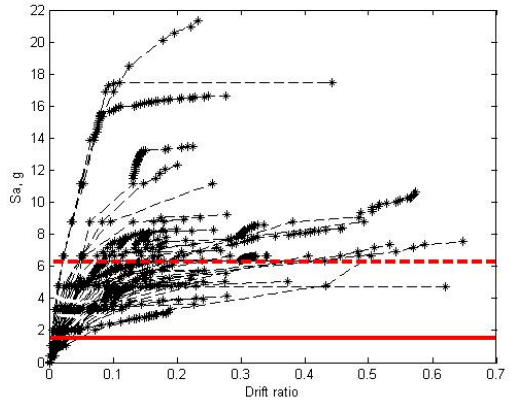

Figure 15. IDA plot for case 4

For this building, the collapse margin ratio is computed to equal 4.17. The adjusted collapse margin ratio (ACMR) is calculated by multiplying SSF by CMR and equals 5.58

7 ONGOING RESEARCH

The ongoing research at the Tokyo Institute of Technology by teh authors is intended to expand the knowledge base for steel SMRF buildings with dampers. The research will closely follow the guidelines and procedures established by ATC 63 (NEHRP 2008).

A total of 9 archetypes are currently under consideration. The basic geometry and distribution of dampers for these models are summarized in Table 1. The selected building models will be regular in plan and elevation with a dominant first mode response. The period of tall buildings is limited to 4 sec in order to limit higher mode effects and ensure sufficient energy is present in the input histories.

Table 1. Archetypes

Archetype	Stories	US Practice	Japan practice
1	2	1 story	
2 & 3	5	3 stories	3 stories
4 & 5	10	5 stories	8 stories
6 & 7	20	10 stories	16 stories
8 & 9	40	20 stories	30 stories

8 DISCUSSIONS

New steel buildings were designed using perfromance based engineering (PBE) and provisions of ASCE 7. SMRFs were used to provide strength; VDDs were used to control story drifts. PBE design using VDDs is superior to the conventional design. The demand on both structural and nonstructural components is reduced.
To date, a refined model of viscous dampers has been formulated that includes damper limit states.

Current research using IDA and limit states of dampers is currently underway. The outcome of this study will provide a more realistic assessment of the performance of moment frames with dampers

As one of the research deliverables, pertinent information will be provided for the designers to assist in seismic design using this approach

9 REFERENCES

ASCE (2005), "ASCE 7-05: Minimum design load for buildings and other structures," American Society of Civil Engineers, Reston, VA

NEHRP (2008), "ATC 63, FEMA P695: Quantification of Building Seismic Performance Factors," Federal Emergency Management Agency, Washington, D.C.

Miyamoto, H.K., and Gilani, A.SJ. (2008), *Design of a new steel-framed building using ASCE 7 damper provisions*, ASCE Structures Congress, Vancouver, BC, SEI institute.

PEER (2005), *Open System for Earthquake Engineering Simulation (OpenSees)*, McKenna, F., Fenves, G., et al, Pacific Earthquake Engineering Research center, University of California, Berkeley. Berkeley, CA.

PEER (2008), *PEER NGA, Records* Pacific Earthquake Engineering Research center, University of California, Berkeley. Berkeley, CA.

Taylor (2008), Personal Communications

Vamvatsikos, D. and Cornell, A.C. (2004) *Applied Incremental Dynamic Analysis*, Earthquake Spectra, Volume 20, No. 2, pages 523–553, Earthquake Engineering Research Institute, Oakland, CA